Three-dimensional Simulation of Heat Transfer and Stresses in a Steel Slab Caster

R. Hardin, P. Du and C. Beckermann
Solidification Laboratory, Department of Mechanical and Industrial Engineering,
University of Iowa, Iowa City, IA 52242, USA
Contact email: becker@engineering.uiowa.edu

Abstract

A three-dimensional simulation model is developed of a continuous steel slab caster for optimizing operating conditions and improving slab quality. The heat transfer simulation includes a multi-component steel solidification model and a method to model the characteristics of every single spray nozzle and roll. The temperature predictions are validated using pyrometer data from an operating caster. The stress simulation is based on a visco-plastic constitutive equation for steel, where the semi-solid mush is treated as a compressible porous medium. The stress predictions show regions in the slab where hot tears and cracks are likely to form.

Keywords. Continuous casting; solidification model; thermo-mechanical stress model; thermal stress model; spray cooling.

Introduction

Caster operation and practice is determined largely by experience, and trial and error. When computer modeling is applied to predict solidification and thermal conditions in the steel, and stresses and potential defects, the caster operating practice can be designed to avoid defects, optimize production and increase energy efficiency. In addition, better product quality, increased plant capacity and reduced production costs result from improved caster operation.

Continuous casting of steel is energy intensive. Based on industrial data [1], it is estimated that a 1% reduction in scrapped production due to casting related defects (such as slab cracking from improper cooling) can result in annual energy savings of 0.14 trillion Btu (0.147 trillion kJ) for one steel plant in our region of the United States. Combining the scrap energy savings with optimized caster operations, such as the ability to direct hot charge steel slabs, a substantially larger energy savings can be achieved.

Continuously cast steel can contain defects, and the quality and material properties of the steel can be less than desired [2]. Defects encountered in continuous casting of steel include cracks [3], inclusions [4], macrosegregation [5], porosity and others [6]. The main goal of our current continuous casting modeling work is extending past efforts to predict macrosegregation and cracking in other casting processes [7-11] to the continuous casting process.

Computer modeling in continuous casting is wide ranging [12-13]. Fundamentally, in order to predict the defects, an accurate heat transfer and solidification model is required. While some computer models focus on the modeling of solidification and stresses in the mold [14] or between a set of rolls [15], our goal is to model the caster in as much detail as possible from the meniscus of liquid in the mold to the cutoff torch. This work builds onto our earlier computer simulation models of continuous casters that included detailed three-dimensional modeling [16,17] and a dynamic spray cooling control algorithm to optimize caster operation under transient conditions (e.g., casting speed changes) [18]. The present model is a three-dimensional model covering the entire steel strand, approximately 20 m long. It has been configured and validated for a different caster setup than used in the earlier models [16,17]. The model is ideal for optimizing caster operation (e.g., adjustment of spray pattern, water flow rates, casting speed, etc.). The model simulates heat transfer in the mold, and due to each roll and spray nozzle in the machine.

Model Description

The three-dimensional steady-state heat transfer and solidification model used here is described in more detail elsewhere [16,17] and only briefly here. The calculation domain extends from the meniscus (liquid top surface in the mold) to a user selectable distance down the caster. In order to reduce computation time, symmetry at the centerline of the slab thickness and/or mid-width can be assumed (or not), and the ability to predict top- and bottom-facing surface temperatures is included in the model. An example temperature distribution for a calculation domain of dimensions 0.15m thick x 2.2 m wide x 20 m long is shown in Figure 1, where symmetry is assumed about the slab mid-width. In this figure, note that different scaling is used in the three directions. In the model, energy transport due to convection is approximated through a thermal conductivity enhancement factor. Axial conduction is not included in this model, since studies with the transient model (where it is included [18]) have shown that axial conduction does not affect the heat transfer and solidification results under normal steady-state operating conditions.

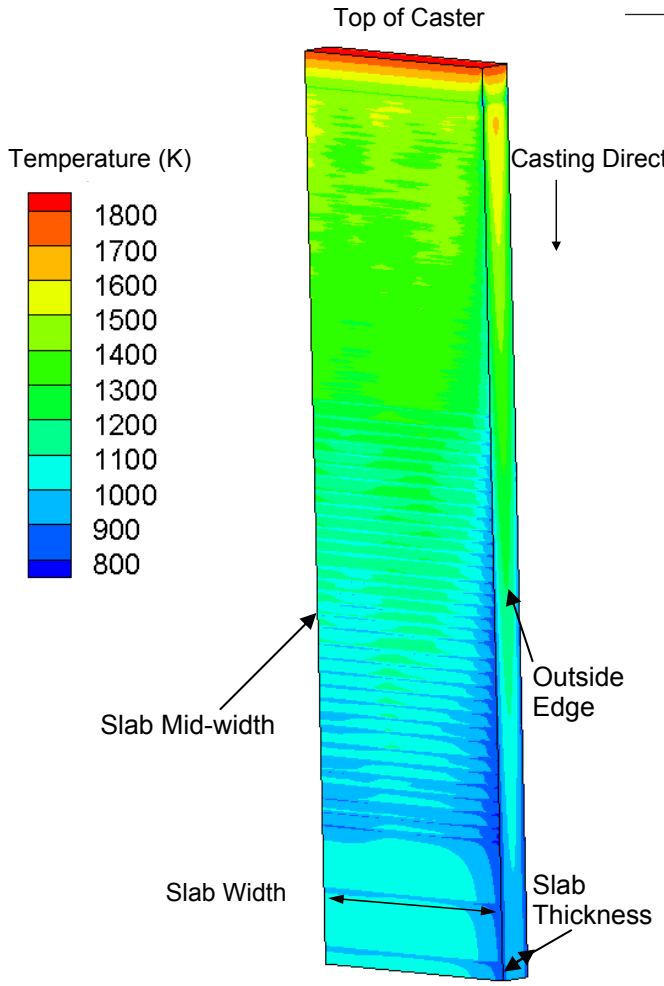

Figure 1 Temperature results on the caster top-facing and outer edge surfaces for a domain of dimensions 0.15m thick x 2.2 m wide x 20 m long. Symmetry is assumed about the slab mid-width. Note the scaling differs in the three directions.

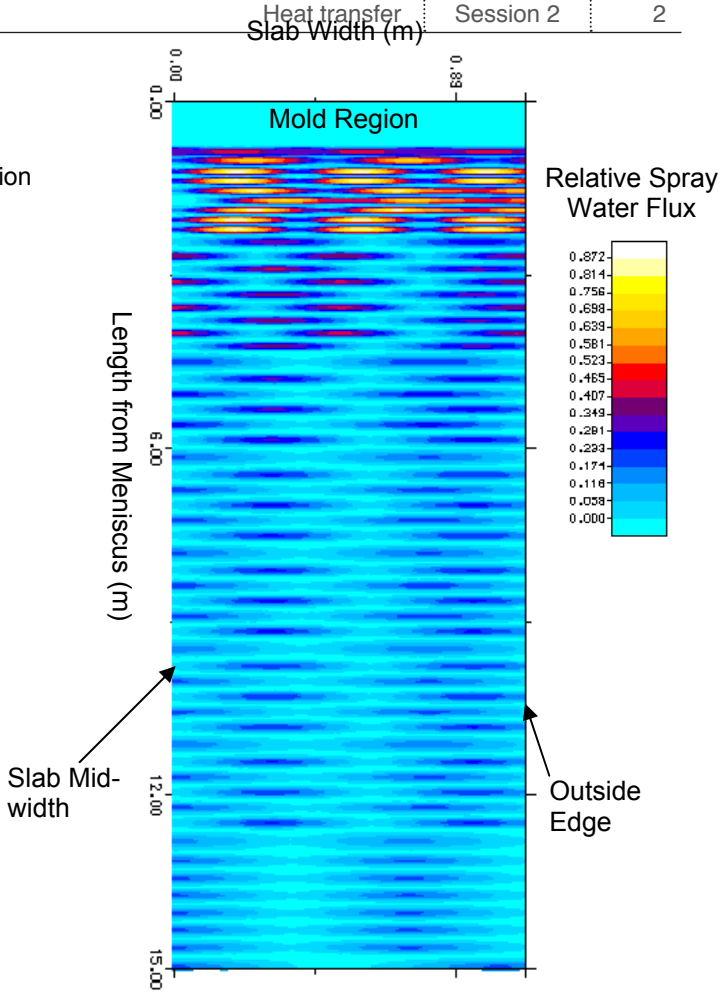

Figure 3 Relative secondary spray cooling water flux (spray flux on surface divided by maximum spray flux) for half of slab width from 0 to 15 m from meniscus. Spray is symmetric about mid-width of slab.

Boundary conditions in the mold are determined from average mold heat flux measurements obtained from online operating data for steady-state casting conditions. Data for the narrow and broad faces of the mold are collected separately. The average mold heat fluxes derived from the data for the narrow and broad faces are then correlated with dwell time in the mold. Dwell time is defined as mold length divided by casting speed. The correlation for the narrow face mold heat flux and the measured data are shown in Figure 2. The error bars are the 95% confidence intervals due to variability in the data over time for a given steady casting sequence. The data and correlation for the broad face mold heat flux were found to be similar to that seen for the narrow face in Figure 2; except that the broad face data showed greater variability and were approximately 15% greater. The model has the option of using either a constant mold heat flux along the mold length, or a prescribed mold heat flux profile along the mold length corresponding to the average mold heat flux.

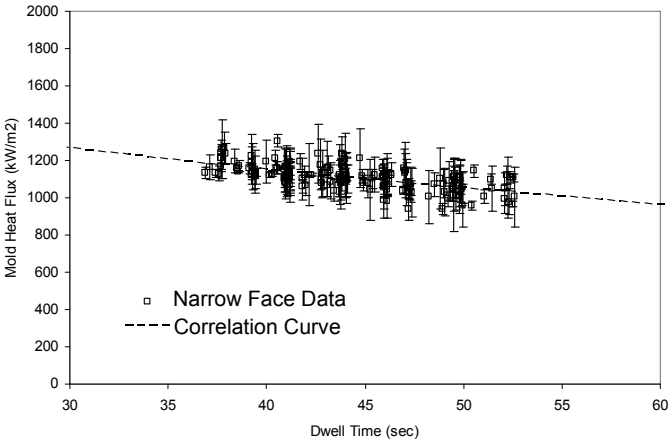

Figure 2 Measured narrow face mold heat flux data and correlation curve used in the model. Error bars denote 95% confidence intervals due to time variability.

Spray cooling, natural convection, roller contact and radiation cooling boundary conditions are used in the model where applicable [16,17]. Considerable effort has been made to realistically model the secondary cooling sprays, as shown in Figure 3. Here a contour plot of the relative secondary spray cooling water flux is shown. The relative flux is the spray flux on surface (i.e. liter/minute/meter^2) divided by the maximum spray flux on the surface. The plot in Figure 3 is over half of

the slab width since the spray is symmetric about the mid-width, and from 0 to 15 m from meniscus. A correlation between the spray heat transfer coefficient and the water spray flux and temperature is used in the model [16,17]. By modeling each spray nozzle used in the caster (top and bottom surface) according to information provided by the caster operators, issues of spray uniformity and overlap can be investigated. The spray nozzle information provided by the caster operators includes: the positions of the nozzles across (width direction) and along the strand (casting direction), the nozzle type, the fan angle and distribution of the spray flux from each nozzle, the height (offset) of the nozzle from the slab surface, and the spray water temperature (from online data). Currently there are six different nozzle assembly types defined in the model, as used in the caster. All-in-all there are 415 nozzles defined for the caster modeled in this paper. Note that higher fluxes are applied nearer the top of the caster as seen in Figure 3, and that there is more spray overlap near the top of the caster. The spray cooling curves defining how the spray water is apportioned to the machine segments (via secondary spray cooling loops or zones), and how spray water within a loop varies with casting speed, was also provided by the caster operators and was built into the model. There are ten spray cooling curves built into the model.

At the rolls, measurements [19,20] have shown that temperature drops of over 200 °C can occur, and heat transfer coefficients can be as high as 2500 ($W/m^2/K$). Here no such measurements have been made on the caster modeled. In lieu of such measurements, the effects of the individual roll contact cooling are resolved using a constant roll heat transfer coefficient of 700 ($W/m^2/K$), and the environmental temperature (used for radiation exchange) is employed instead of the actual roll surface temperature, again due to lack of measurements. This environmental temperature is a model parameter, but is nominally set to 34 °C. Although approximate, this combination of heat transfer boundary parameters at the rolls produces temperature drops at the roll contacts as measured in the literature for similar casting machines. Consult references [16] and [17] for additional details on the model and boundary conditions used.

This model differs from many slab caster models in that the latent heat development and solidus temperature is computed according to the cooling conditions within a given computational cell. This is done by inputting the composition of the steel and modeling the microsegregation during the solidification process accordingly [16,17]. Finally, the caster solidification model is a self contained package consisting of a preprocessor for setting up casting conditions (complete with property database and property visualization software), and a postprocessor to visualize temperature and solid fraction contours, and profiles, anywhere in the cast slab. The water spray flux on the top and bottom facing surfaces may also be visualized.

Currently, the caster solidification and the stress models are uncoupled. The caster heat transfer model is run first, and then the temperature and solid fraction results are exported to the commercial finite element package ABAQUS to predict the stress development in the slab. Specifically, at axial positions down the three-dimensional steady-state caster model the cross-section data at thickness and width positions are mapped onto the nodes of a two-dimensional finite element mesh. This two-dimensional domain is then used in a Lagrangian frame of reference to compute the stress development over the time that corresponds to the axial position from meniscus. The element type used is CPEG4 (a 4-node bilinear generalized plane strain quadrilateral element). If uniformly spaced, approximately 1000 axial slices are required over a 20 m long caster to capture the roll contacts.

The stress results presented in this paper consider only thermal induced stresses. The stress modeling used in ABAQUS employs a user material model (UMAT subroutine), applying a visco-plastic constitutive model with damage to compute the solid deformation [9-11]. Damage created by mechanically induced voiding is used as a defect indicator. The boundary conditions used in the stress calculations presented here employ symmetry about the slab mid-width line, and the mid-thickness point on this plane is pinned.

Model Results

The model was calibrated by comparing predicted model temperatures with measured temperatures. In this calibration, adjustments were made to the heat transfer correlation used in the spray cooling [16,17] based on their sensitivity to the model output until the best agreement between measured and predicted temperatures was obtained. The temperature measurements were made at four pyrometers installed on the caster top-facing surface. As shown in Figure 4, three were located at 6.15 m from meniscus (between segments 2 and 3) and one was at 12.8 from meniscus between segments 6 and 7. The pyrometer positions across the slab width were: pyrometer 1 at the slab mid-width, pyrometers 2 and 4 are offset by 11 cm from the slab mid-width, and pyrometer 3 is offset by 17 cm from the slab mid-width. Only measured temperatures for steady-state casting conditions (defined as casting variables being constant for at least 20 minutes) were compared with model results. Based on their variation with time, 95% confidence intervals were established for the temperature measurements. For the predicted temperatures, it was assumed the true positions of pyrometers on the caster were not known within ±4 cm

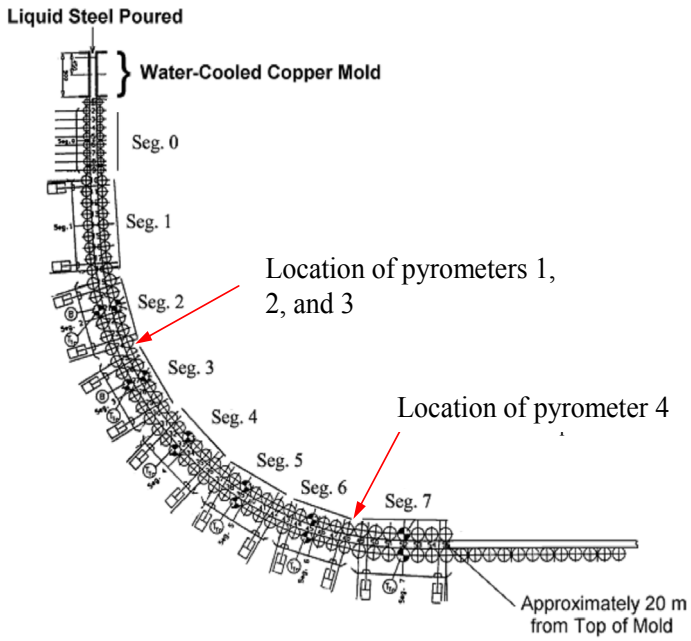

Figure 4 Positions of pyrometers along the casting direction used to measure surface temperatures for caster model verification Location of pyrometers 1, 2 and 3 is 6.15 m from meniscus, and pyrometer 4 is 12.79 m.

about the positions reported earlier. In this 8 cm square box the mean and confidence interval for the predicted temperature values were determined.

From the online data collected over a six week period, 29 sets of steady-state data were used for the model calibration. After the model calibration, all 29 cases were run and a benchmark comparison was made between the measured and predicted temperatures. The comparison for one case is shown in Figure 5.

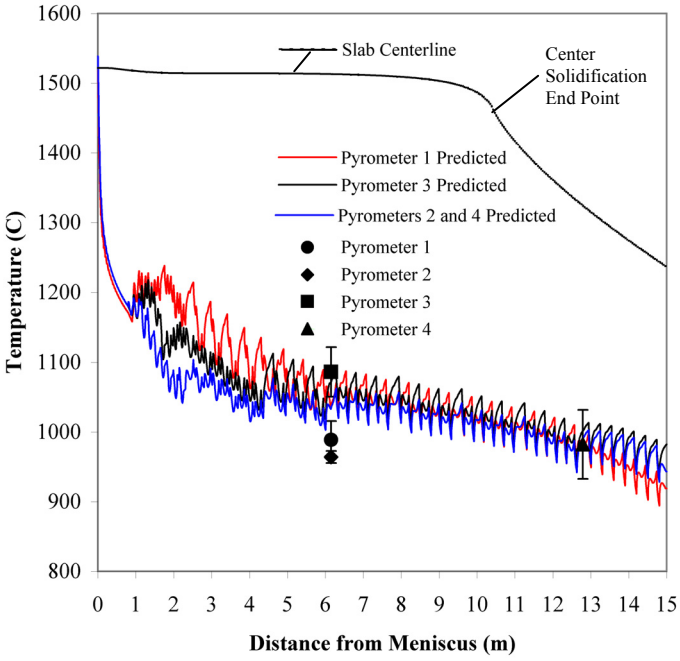

Figure 5 Predicted temperature profiles along caster length at the three width positions where the pyrometers are located, and at the center of the slab. Pyrometer error bars are 95% confidence intervals for the measurements.

Here the predicted temperature profiles along caster length at the three width positions where the pyrometers are located are shown. Also the temperature at the center of the slab is shown so the solidification end point may be visualized. Note that the solidification end point is not necessarily at the slab centerline/middle thickness point due to the realistic and non-uniform spray cooling model. The comparison between measured and predicted temperatures for all 29 cases is presented in Figure 6, where the dashed line corresponds to perfect agreement between them. Note that two pyrometer 3 measurements are circled, and these appear to be outliers where the temperature is under predicted. Examining these cases, their slab widths are narrow, and the pyrometer location is quite close to the corner of the slab. At this location the uncertainty of the true pyrometer position must be eliminated if an accurate comparison is to be made, since the temperature variation near the slab corners is large. This issue will be investigated.

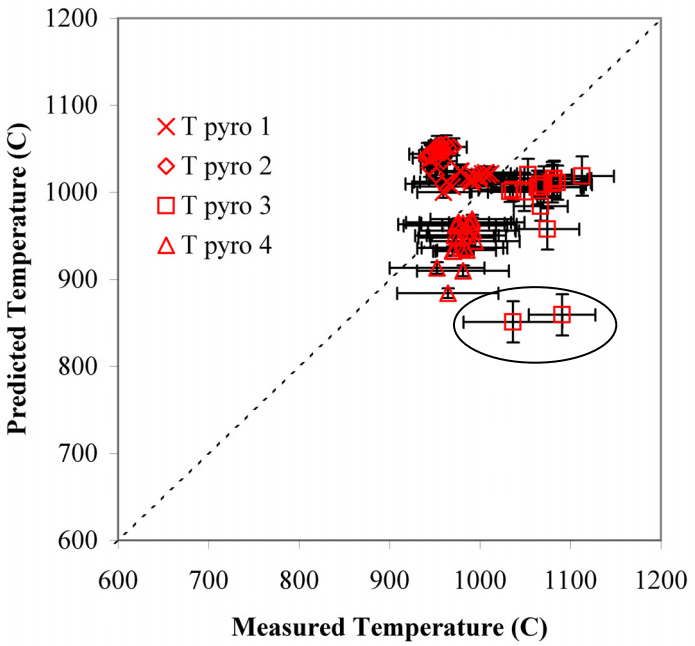

Figure 6 Predicted versus measured temperatures after model calibration. This comparison shows good agreement and model validation.

Currently, the prediction of longitudinal cracking is the primary object for the stress model. These can develop from large hoop stresses pulling across the slab width. In the caster modeled there are conditions and alloy grades where these sometimes appear, usually near the center of the slab broad face. Using the model, conditions where these cracks occur are simulated and compared with simulations for conditions where the cracks do not occur. The objective is to develop a criteria or indicator to predict cracks (similar to [9]). Here example results in the slab cross section at 6.15 m from meniscus are shown in Figure 7. The temperature and solid fraction

used in the thermal stress model are shown in Figures 7 (a) and (b), respectively. Note that half the slab width is simulated. In Figure 7 (c) and (d) the Von Mises stress and hoop stress are shown, respectively. The hoop stress is most probably responsible for longitudinal crack formation. In Figure 7 (d), note that the stresses are in tension at/near the surface, and are

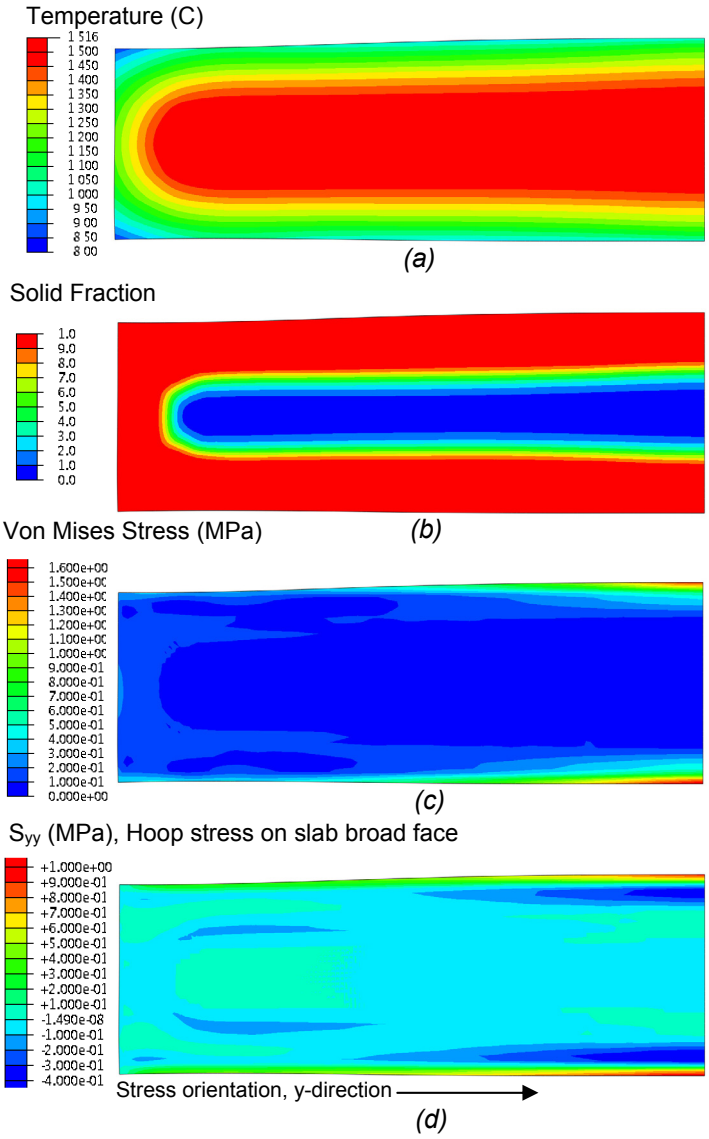

Figure 7 Predictions in cross section at pyrometers 1 to 3 at 6.15 m from meniscus: (a) temperature, (b) solid fraction, (c) Von Mises stress, and (d) hoop stress or stress responsible for longitudinal cracks.

in compression beneath the surface. If these tensile stresses are large enough, relative to the material's yield strength, a longitudinal crack will form.

Conclusion

The continuous steel casting process can be improved through advanced computer modeling by predicting the cause of casting defects and optimizing caster operating conditions. The model presented here gives good agreement between measured and predicted temperatures. The model is developed with a user friendly graphical user interface and post-processor. This makes the model useful to users with a wide variation of technical expertise, ranging from plant operators to research engineers. Simulations with the stress model predict stress hot spots at locations where longitudinal cracks are observed, but work remains to develop the crack prediction criteria.

Acknowledgements

This work was conducted through funding from the Iowa Energy Center under grant number 09-02. The authors gratefully acknowledge this support. In addition, the authors thank the SSAB Montpelier, Iowa Steelworks for their participation in the project and online data for model validation.

References

[1] American Iron and Steel Institute: Saving One Barrel of Oil per Ton: A New Roadmap for Transformation of Steelmaking Process; available at http://www.steel.org/, October 2005.

[2] Brimacombe, J.K.: The Challenge of Quality in Continuous Casting Processes; Metall. Mater. Trans. A, Vol. 30A, 1999, P. 1899-1912.

[3] Brimacombe, J.K.; Sorimachi, K.: Crack Formation in the Continuous Casting of Steel; Metall. Mater. Trans. B, Vol. 8B, 1977, P. 489-505.

[4] Zhang, L.; B.G. Thomas: Inclusions in Continuous Casting of Steel; XXIV National Steelmaking Symposium, Nov. 26-28, 2003, P. 138-183.

[5] Beckermann, C.: Modelling of Macrosegregation: Applications and Future Needs; Int. Mater. Rev., Vol. 47, 2002, P. 243-261.

[6] W.R. Irving: Continuous Casting of Steel, London, UK: Inst. of Materials, 1 Carlton House Terrace, 1993, P. 93-155.

[7] Schneider, M.C.; Beckermann C.: Formation of Macrosegregation by Multicomponent Thermosolutal Convection during Solidification of Steel; Metall. Mater. Trans. A, Vol. 26A, 1995, P. 2373-2388.

[8] Gu, J.P.; Beckermann, C.: Simulation of Convection and Macrosegregation in a Large Steel Ingot; Metall. Mater. Trans. A, Vol. 30A, 1999, P. 1357-1366.

[9] Monroe, C.; Beckermann, C.: Development of a Hot Tear Indicator for Steel Castings; Mater. Sci. Eng. A, Vol. 413-414, 2005, P. 30-36.

[10] Monroe, C.; Beckermann, C.: Simulation of Hot Tearing and Distortion During Casting of Steel: Comparison with Experiments; in Proceedings of the 60th Technical and Operating Conference, SFSA, Chicago, IL, 2006.

[11] Pokorny, M.G.; Monroe, C.A.; Beckermann, C.; Zhen, Z.; Hort, N.: Simulation of Stresses During Casting of Binary Magnesium-Aluminum Alloys; Metall. Mater. Trans. A, Vol. 41A, 2010, P. 3196-3207.

[12] Thomas, B.G.: Modeling of the Continuous Casting of Steel: Past, Present and Future; 59th Electric Furnace Conference Proceedings, ISS, Warrendale, PA, 2001, P. 3-30.

[13] Thomas, B.G.: Recent Advances in Computational Modeling of Continuous Casting of Steel; Scanmet II Conference, MEFOS, Vol. 1, 2004, P. 243-252.

[14] Koric, S.; Hibbeler, L.; Thomas, B.G.: Explicit Coupled Thermo-Mechanical Finite Element Model of Steel Solidification; Int. J. Num. Meths. Engineering, Vol. 78, 2009, P. 1-31.

[15] Camporredondo, S. J.; Castillejos, E. A.; Acosta, G. F.; Gutierrez, M. E.; Herrera, G. M.: Analysis of thin-slab casting by the compact-strip process: Part II. Effect of operating and design parameters on solidification and bulging; Metall. Mater. Trans. B, Vol. 35, No. 3, 2004, P. 561-573.

[16] Hardin, R.A.; Shen, H.; Beckermann, C.: Heat Transfer Modeling of Continuous Steel Slab Casters Using Realistic Spray Patterns; in Modeling of Casting, Welding and Advanced Solidification Processes IX, eds. P.R. Sahm et al., Shaker Verlag, Aachen, Germany, 2000, P. 729-736.

[17] Shen, H.F.; Hardin, R.A.; MacKenzie, R.; Beckermann, C.: Simulation using Realistic Spray Cooling for the Continuous Casting of Multi-Component Steel; J. Materials Science and Technology, Vol. 18, 2002, P. 311-314.

[18] Hardin, R.A.; Liu, K.; Kapoor, A.; Beckermann, C.: A Transient Simulation and Dynamic Spray Cooling Control Model for Continuous Steel Casting; Metall. Mater. Trans. B, Vol. 34B, 2003, P. 297-306.

[19] El-Bealy, M.; Leskinen, N.; Fredriksson, H.: Simulation of Cooling Conditions in Secondary Cooling Zones in Continuous Casting Process; Ironmaking and Steelmaking, 22 (3), 1995, P. 246-255.

[20] York, R.; Spitzer, K.H.: Heat Transfer in the Secondary Cooling Region on Continuous Casting Machines", Solidification Processing 1997: Proceedings of the 4th Decennial International Conference on Solidification Processing, Dept. of Eng. Mat., University of Sheffield, 1997, P. 163-165.